

Detuning-dependent Properties and Dispersion-induced Instabilities of Temporal Dissipative Kerr Solitons in Optical Microresonators

Erwan Lucas, Hairun Guo, John D. Jost, Maxim Karpov, and Tobias J. Kippenberg*
École Polytechnique Fédérale de Lausanne (EPFL) – Institute of Physics, Lausanne, CH-1015, Switzerland.
(Dated: November 29, 2018)

Temporal-dissipative Kerr solitons are self-localized light pulses sustained in driven nonlinear optical resonators. Their realization in microresonators has enabled compact sources of coherent optical frequency combs as well as the study of dissipative solitons. A key parameter of their dynamics is the effective-detuning of the pump laser to the thermally- and Kerr-shifted cavity resonance. Together with the free spectral range and dispersion, it governs the soliton-pulse duration, as predicted by an approximate analytical solution of the Lugiato-Lefever equation. Yet, a precise experimental verification of this relation was lacking so far. Here, by measuring and controlling the effective-detuning, we establish a new way of stabilizing solitons in microresonators and demonstrate that the measured relation linking soliton width and detuning deviates by less than 1% from the approximate expression, validating its excellent predictive power. Furthermore, a detuning-dependent enhancement of specific comb lines is revealed, due to linear couplings between mode-families. They cause deviations from the predicted comb power evolution, and induce a detuning-dependent soliton recoil that modifies the pulse repetition-rate, explaining its unexpected dependence on laser-detuning. Finally, we observe that detuning-dependent mode-crossings can destabilize the soliton, leading to an unpredicted soliton breathing regime (oscillations of the pulse) that occurs in a normally-stable regime. Our results test the approximate analytical solutions with an unprecedented degree of accuracy and provide new insights into dissipative-soliton dynamics.

I. INTRODUCTION

Dissipative Kerr-cavity Solitons (DKS) are self-localized pulses of light that can be excited in coherently-driven nonlinear optical resonators. Following earlier studies of externally-induced dissipative solitons in fiber cavities [1], they were shown to spontaneously form in microresonators [2]. From an applied perspective, DKS generation in microresonators enables high-repetition rate sources of ultrashort pulses, producing coherent, broadband optical “Kerr” frequency combs [3]. Kerr frequency combs are generated by coupling a strong continuous wave laser into a nonlinear microresonator that converts the initial frequency into a set of equidistant comb lines via a cascade of parametric effects [4]. With proper tuning of the pump laser, these processes result in the formation of DKS in the cavity sustained via the double balance between cavity loss and parametric gain, as well as dispersion and Kerr nonlinearity [1, 2, 5–7]. These DKS-based frequency combs have been demonstrated in several microresonator platforms, enabling on-chip photonic integration [2, 8–10]. Compared to other optical frequency comb platforms, DKS combs extend the repetition rate to the microwave and milli-meter wave domain, while simultaneously providing wide bandwidth and compact form factor. They have already been successfully used for coherent terabit communications [11], microwave-to-optical phase coherent links [12–14], and the generation of low noise microwaves [15]. The interplay of the fundamental aspects of soliton physics and

their applications has shown the suitability of the microresonator platform to study soliton properties. A recent demonstration evidenced how soliton Cherenkov radiation in a dispersion-managed resonator [8, 16, 17] can extend the frequency comb bandwidth, enabling self-referencing without external broadening [14].

Fundamentally, the dynamics of the DKS rely on the resonator properties and two external parameters of the pump laser: the power and the detuning to the pumped resonance. An analytical estimate [2, 18] predicts that the soliton duration (and thus the comb bandwidth) only depends on the resonator free spectral range, dispersion, and detuning. While the former two parameters are readily accessible and measurable with high precision, the detuning of the nonlinear system is more challenging to determine, in particular since microresonators are susceptible to thermal nonlinearities [19, 20]. Here, we apply a recently introduced method [21, 22] enabling detuning measurement, to carry out a controlled study of the effect of the detuning on the properties of a single soliton in a crystalline magnesium fluoride (MgF_2) resonator, and perform a careful comparison of the measurements to the theoretical predictions. This is achieved via a feedback-stabilization of the detuning parameter, which ensures the stability over the measurement duration and enabled long-term soliton stabilization. The results show very good agreement between the soliton pulse bandwidth and the analytical approximation that deviate by less than 1%. Local features in the resonator dispersion caused by coupling of other spatial mode families induce detuning-dependent spectral features, which are shown to cause a soliton recoil, and affect the repetition rate as well as the total comb power. Unexpectedly, mode crossings are further shown to alter the soliton stability,

* Corresponding author: tobias.kippenberg@epfl.ch

leading to a “breathing” regime in which the soliton amplitude and width oscillate. This soliton breathing occurs at a detuning range, where the solitons are expected to be stable. Beyond elucidating the detuning dependence of temporal solitons, this work, to the best of the authors knowledge, constitutes a direct experimental verification of the DKS models with an accuracy that has not been attained in previous studies of this class of solitons.

II. ANALYTICAL DESCRIPTION

The complex dynamics of a continuous-wave (CW) laser-driven nonlinear optical microresonator can be described both in the frequency and time domains, via coupled mode equations [23] or via a spatiotemporal description [24, 25]. In the time domain, the equation of motion for the envelope of the cavity field is given by:

$$\frac{\partial A}{\partial t} = -\left(\frac{\kappa}{2} + i\delta\omega\right)A + i\frac{D_2}{2}\frac{\partial^2 A}{\partial \phi^2} + ig_0|A|^2A + \sqrt{\frac{\eta\kappa P_{in}}{\hbar\omega_0}} \quad (1)$$

where κ denotes the loaded resonator linewidth ($Q = \omega_0/\kappa$, loaded quality factor), $\eta = \kappa_{ex}/\kappa$ the coupling coefficient, P_{in} the pump power, ω_0 the pumped resonance frequency (thermally shifted) and $\delta\omega = \omega_0 - \omega_p$ is the detuning of the pump laser to this resonance. The dispersion of the resonator is described by expressing the resonance frequency as a function of the mode number μ (relative to the pumped mode) as $\omega_\mu = \omega_0 + \mu D_1 + \mu^2 D_2/2$, where D_1 correspond to the FSR in rad/s and D_2 relates to the GVD parameter β_2 ($D_2 = -\beta_2 D_1^2 c/n_0$). The non-linearity is described via the (per photon Kerr frequency shift) coefficient $g_0 = \hbar\omega_0^2 cn_2/n_0^2 V_{\text{eff}}$, with the refractive index of MgF₂ n_0 , nonlinear refractive index n_2 , and the effective cavity nonlinear volume $V_{\text{eff}} = A_{\text{eff}}L$ (A_{eff} is the effective nonlinear optical mode area and L the circumference of the cavity). Under suitable normalization, the above equation has been shown to be equivalent to the Lugiato-Lefever equation (LLE) that originally described spatial pattern formation in diffractive cavities [2, 6, 24, 26]. For anomalous group velocity dispersion ($D_2 > 0$), there exist stable solutions consisting of DKS on top of a weak continuous field. The approximate expression for the soliton component yields a hyperbolic secant pulse such that for a single soliton in the microresonator, the comb power spectral envelope follows a sech^2 spectral profile [2, 18]:

$$P(\mu) \approx \frac{\pi}{2} \frac{\eta}{Q} \frac{D_2}{D_1} \frac{n_0 A_{\text{eff}}}{n_2} \text{sech}^2\left(\frac{\pi\tau}{2}\mu\omega_r\right), \quad (2)$$

$$\tau \approx \frac{1}{D_1} \sqrt{\frac{D_2}{2\delta\omega}}, \quad (3)$$

where ω_r is the comb repetition rate and τ the pulse duration (corresponding pulse FWHM $\tau_{\text{FWHM}} =$

$2\text{acosh}(\sqrt{2})\tau$). Therefore, following this approximation, the soliton pulse duration is only determined by *three frequencies*, while the other cavity properties determine the soliton’s power levels.

Eq. (3) is at the core of several recent works on soliton, as in [9], where it was employed to replace $\delta\omega$ dependencies with τ . A direct verification of this approximation with experiment would further consolidate the validity of such approach. Surprisingly, although simulations of the LLE and comparisons to soliton experiments have rapidly advanced in recent years, the fundamental test of (3) in microresonators has not been directly performed, due to lack of direct access to $\delta\omega$ in the driven nonlinear system in the presence of solitons. In microresonators, photo-thermal and Kerr effects play a key role [19]. When tuning the laser across a resonance to obtain a soliton state, the thermal effect shifts the cavity resonance from its original cold position [2, 8], making it difficult to precisely infer the *effective* laser detuning from this ‘hot’ cavity resonance.

In addition, this detuning not only determines the soliton duration, but also if the soliton can be sustained. The soliton is indeed supported in the cavity over a limited range of effective red-detuning ($0 < \delta\omega < \delta\omega_{\text{max}}$) referred to as soliton existence range. Therefore, thermal drifts of the microresonator cavity can cause the effective detuning to walk outside of these limits, leading to the decay of the soliton state.

III. RESULTS

A. Effective detuning probing and stabilization of a dissipative Kerr soliton state

In order to study the soliton properties as a function of the effective detuning, this parameter must be measured, stabilized, and tuned in a controlled way. We recently demonstrated a way to probe the effective detuning within the soliton state [22], akin to techniques employed in ultrafast lasers [27, 28]. The underlying idea is to frequency-sweep weak phase-modulation sidebands imprinted onto the pump laser and record the resulting amplitude modulation of the optical power coming out of the cavity. The sweep is generated with a Vector Network Analyzer (VNA) and converted to a phase modulation on the laser with an Electro-Optical Modulator (EOM). After the resonator, the corresponding amplitude modulation is recorded on a photodiode and demodulated by the VNA (see Fig. 1a). When solitons propagate in the cavity, the system’s transfer function exhibits a *double-resonance* feature, related to the strong bistability of the cavity that supports both a weak CW background and high intensity solitons. A first small peak at low modulation frequencies is observed (*S*-resonance) that relates to a resonance of the soliton and is weakly dependent on the detuning. A second stronger peak (*C*-resonance) is also measured, whose frequency corre-

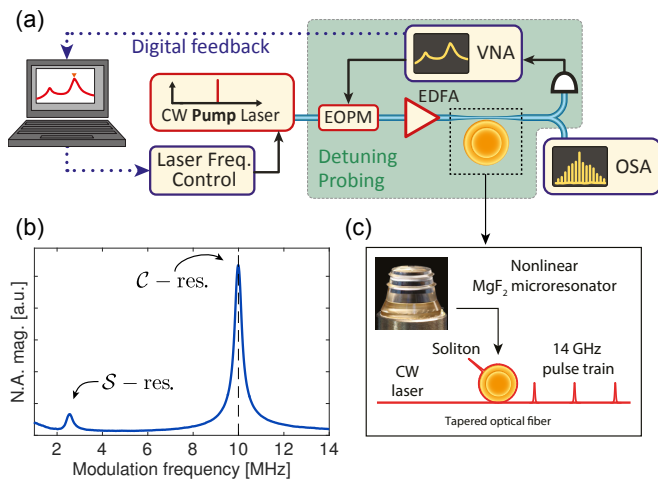


Figure 1. Kerr comb generation, probing and stabilization. (a) Experimental setup: Vector Network Analyzer (VNA), Electro-Optic Phase Modulator (EOPM), Erbium Doped Fiber Amplifier (EDFA), Optical Spectrum Analyzer (OSA). (b) Double-resonance cavity transfer function in the soliton state, as measured on the VNA. The frequency of the \mathcal{C} -resonance indicates the pump-resonator detuning. (c) Principle of microresonator frequency comb generation and formation of dissipative Kerr solitons.

sponds to the effective detuning $\delta\omega$ of the pump laser to the optical resonance of the microresonator, when $\delta\omega \gg \kappa$. The soliton existence range can be determined easily with this probing technique by detuning the laser until the soliton is lost. We measured it to range from $\delta\omega/2\pi \sim 2$ MHz to ~ 30 MHz, which corresponds to an effective laser-cavity detuning of $\delta\omega/\kappa \sim 160$ times the resonance linewidth. This is enabled by the strong pumping of the resonator, that is ~ 140 times above the parametric threshold ($P_{in} \approx 215$ mW, intrinsic linewidth $\kappa_0/2\pi \approx 100$ kHz, $\eta \approx 0.43$) [23].

We implemented a digital feedback-stabilization of the effective detuning, as shown in Fig. 1a. The response of the system is measured with the VNA (sweep time ~ 100 ms) and recorded with a computer. The detuning value is identified by detecting the \mathcal{C} -resonance frequency with a peak detection algorithm, and the program determines the required feedback to apply to the pump laser frequency to stabilize the detuning to a given value. The overall feedback is slow (~ 10 Hz) but sufficient to compensate the thermal drift, which is the main source of variations. This method enabled the long term stabilization of a single soliton in the crystalline microresonator over 15 h as presented on Figure 2. Over this period, the laser frequency was adjusted by more than 350 MHz, which represents over ten times the existence range of the soliton. The active compensation maintained the effective detuning fixed at 10 MHz and stabilized the comb bandwidth (Fig. 2c,e). However, the parameters of the resulting frequency comb are not stabilized, since the cavity FSR drifts thermally and so does the pulse repetition

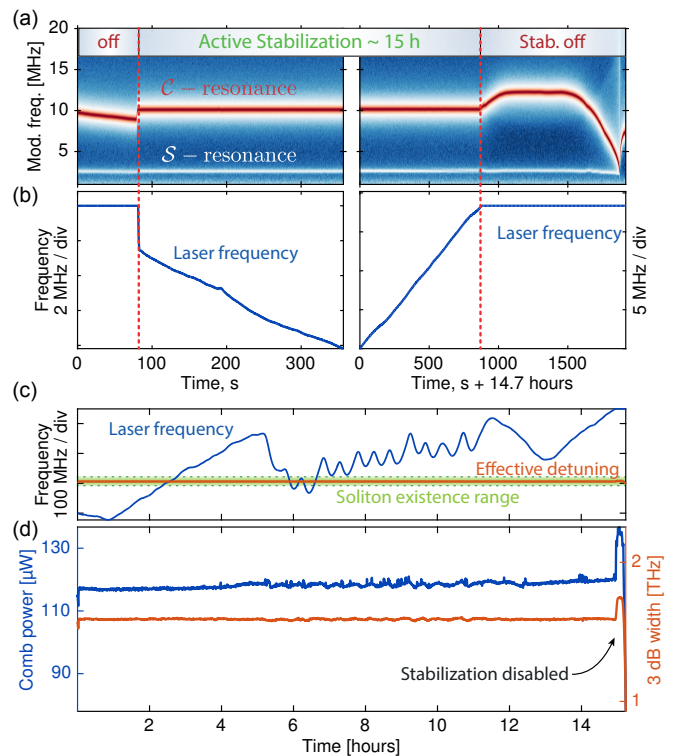


Figure 2. Effective detuning stabilization of a dissipative Kerr soliton state. (a-b) Close-in view of the lock enabling and disabling. The colormaps in (a) show the concatenated set of acquired VNA traces used to determine the detuning. The plots in (b) trace the pump frequency. If the lock is enabled, the laser is tuned to keep the effective detuning at a fixed value. When the lock is disabled, the laser frequency is fixed, but the soliton is lost after 17 min. (c-d) Stabilization and continuous soliton measurement over 15 h. (c) The blue line indicates the evolution of the pump laser frequency when tracking the microresonator resonance, which is measured by counting the heterodyne beat of the pump with an ultra-stable laser. The temperature drifts of the microresonator cavity are the main source of variations and the slow oscillations are caused by the air conditioning. The red line indicates the stabilized effective detuning (at 10 MHz) that remains within the soliton existence range. (d) The comb power and the 3 dB bandwidth (obtained by fitting the optical spectra) are stabilized when the laser compensates the drifts.

rate. To highlight the effect of the stabilization, the lock was disabled on purpose after ~ 15 h and the thermal drifts caused the comb properties to drift until the soliton state decayed after 17 min.

B. Study of the detuning-dependent dissipative Kerr soliton duration

In order to study the dependence of the soliton on the effective detuning, this parameter was swept by changing the set-point in the computer. Figure 3a shows a

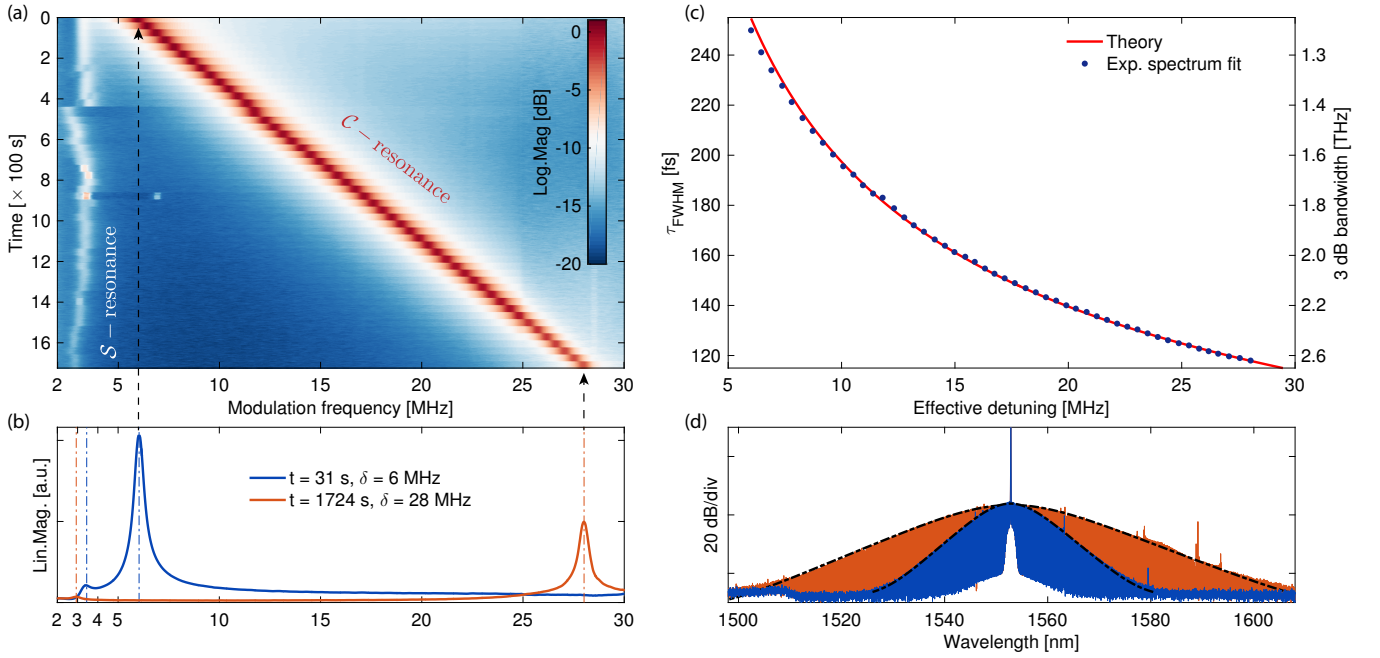


Figure 3. **Tuning of the effective detuning and evolution of the soliton duration.** (a) Map showing the evolution of the modulation response (log scale) as the effective detuning is swept. The detuning is stabilized at each step. (b) The observed VNA traces at the extrema of the effective detuning ($\delta\omega$). (c) The measured soliton full width at half maximum (derived from a sech^2 fit) is plotted versus the detuning (blue dots) with comparison to the expression in Eq. (3) (red line). (d) Corresponding spectra at the limits of the sweep. As expected, the comb bandwidth increases with larger effective detuning. The black lines mark a sech^2 fit of the combs.

sweep of the effective detuning from 6 to 28 MHz, in 50 steps. At each step, once the detuning was stabilized, an optical spectrum was acquired (OSA scan time ~ 30 s) and the comb average power (after suppressing the pump with a narrowband fiber Bragg grating) was measured with a photodiode, before moving to the next detuning value. At the same time, ω_r was measured with a frequency counter after photo-detection and down-mixing. The overall measurement duration is ~ 30 min and the active detuning stabilization is required to counteract the environmental drifts. Each optical spectrum was fitted with the following expression:

$$A \text{sech}^2 \left(\frac{\mu\omega_r - \Omega}{B} \right), \quad (4)$$

where μ is the relative mode number, ω_r the repetition rate of the comb, $B = 2/(\pi\tau)$ the bandwidth, A the power of the central comb line and Ω the spectral shift of the comb centroid from the pump.

The presented method enables a precise comparison between the measured comb properties and the theoretical predictions. The dispersion properties of the resonator were measured experimentally via frequency comb assisted scanning laser spectroscopy [29, 30] and shown in Figure 5d. (the corresponding dispersion parameters are $D_1/2\pi = 14.094$ GHz, $D_2/2\pi = 1.96$ kHz, $D_3/2\pi = -1.39$ Hz). The soliton spectral bandwidth (and deduced pulse duration) obtained experimentally

is compared with the approximate expression Eq. (3), using the measured dispersion and detuning parameters (Fig. 3a). We observe an excellent agreement of the two curves (normalized RMS deviation of 0.8 %) supporting the validity of the approximation. The results also show that the soliton duration can be tuned by more than a factor of 2 by changing the detuning.

C. Study of the detuning-dependent mode crossings and soliton recoil

The relation between average power of the comb and detuning is obtained by integrating Eq. (2):

$$\bar{P} = \frac{2\eta A_{\text{eff}} n_0 \kappa}{n_2 \omega_0 D_1} \sqrt{2D_2 \delta\omega}. \quad (5)$$

The evolution of the measured comb power, shown in Figure 4a, follows the trend of the previous equation, but significant discrepancies are observed at some detuning values, such as for $\delta\omega/2\pi = 12$ MHz, where a large spike in the comb power is measured. Integrating the fit expression (4) reveals that the power in the soliton is reduced at these points (blue dots in Fig. 4a). The corresponding spectrum exhibits specific comb lines that are strongly enhanced (Fig. 4b). This effect is typically caused by avoided mode crossing, where the coupling between two spatial mode families causes a local disruption

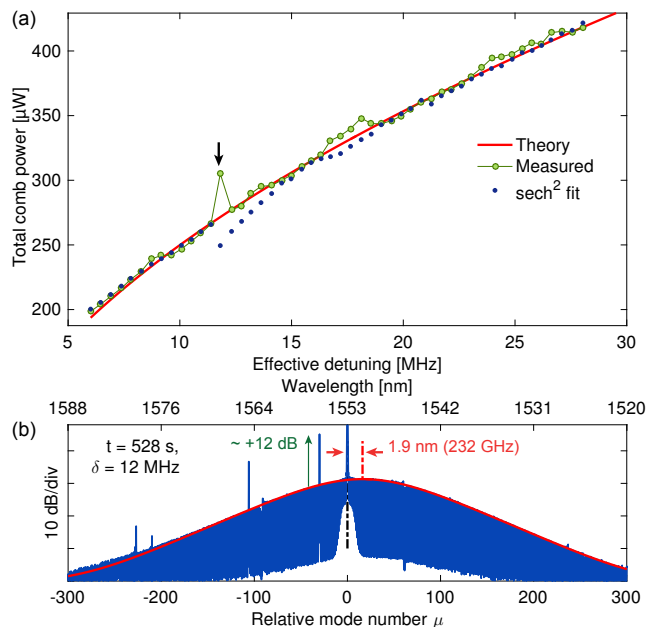


Figure 4. **Evolution of the soliton power.** (a) Evolution of the measured comb power with the effective detuning (green dots), compared to Eq. (5), and the estimated power in the soliton component (blue dots, derived from the sech^2 fit). (b) Comb spectrum corresponding to the arrow in a. The black dashed line marks the pump position ($\mu = 0$). Two strong avoided mode crossing are visible at $\mu = -31$ and $\mu = -106$, and induce a shift of the sech^2 centroid from the pump toward shorter wavelength, marked by the red arrows.

in the resonator dispersion, leading to a modification of the phase matching condition between the pump to a sideband mode. This is associated with an enhancement or suppression of the comb generation at the crossing position [29, 31, 32]. The excess power in certain lines (spikes) makes the frequency comb asymmetric, which induces a recoil – i.e. a shift in the soliton center frequency with respect to the pump – in the opposite direction, in order to keep the spectral center of mass invariant [17, 33, 34]. In the time domain, the spike beats with the pump laser, leading to an oscillating intracavity background. The soliton(s) are then trapped on this oscillating pattern, creating a bound state [35].

The evolution of the mode crossing features with the laser detuning is further investigated in Figure 5. Interestingly, the measured dispersion of the mode family supporting the soliton does not exhibit strong disruptions (see Fig. 5d), instead we observe periodic crossings with a mode family having a different FSR. We detect the mode crossings features in the comb spectrum by first subtracting the sech^2 fit, to estimate the power deviation ΔP of each comb line (see Fig. 5a). The power deviation of the concerned comb lines evolves with the detuning, abruptly transitioning to being enhanced or suppressed over a small range of detuning, as illustrated in Figure 5b. The deviations in the residual ΔP are detected, and

reported on Figure 5c. We observe here that the spectral location of the mode crossing features in the comb spectrum is fixed and match those of the modal deviations in the measured dispersion. We also note a clear correlation between strongly enhanced comb lines and the shift of the soliton centroid, that recoils away from these lines. To further check the appearance of avoided mode crossings induced recoil, we estimate the expected soliton recoil $\tilde{\Omega}$ based on the conservation of the spectral center of mass:

$$\int_{-\infty}^{+\infty} \mu A \text{sech}^2 \left(\frac{\mu \omega_r - \tilde{\Omega}}{B} \right) d\mu + \sum_{\mu} \mu \Delta P = 0$$

$$\Leftrightarrow \tilde{\Omega} = -\frac{\omega_r^2}{2AB} \sum_{\mu} \mu \Delta P, \quad (6)$$

This estimate is plotted in Figure 5e, together with the fitted parameter Ω in (4), and an overall agreement is found between these two values. It is interesting to note that the soliton experiences a spectral recoil toward higher optical frequencies, which is opposite to the so far reported frequency shifts observed in microresonators in amorphous silica or silicon nitride. Indeed, in these platforms, the first order Raman shock term dominates and systemically shifts the frequency comb toward lower frequencies, and can compensate the recoil induced by a dispersive wave [9, 36]. The absence of Raman self-frequency shift is expected in crystalline MgF_2 platforms, where the Raman gain is spectrally narrow [37].

The recoil on the soliton implies a change in the soliton's group velocity and thus a modification of the comb repetition rate, according to $\omega_r = D_1 + \Omega D_2/D_1$ [38], similar to the Gordon–Haus effect in mode-locked lasers [39, 40]. This is verified in Figure 5f, where the change in the repetition rate frequency is plotted as a function of the measured recoil and fitted with a linear model. The intercept matches the free spectral range $D_1/2\pi$ and the slope yields $D_2/2\pi = 1.72 \pm 0.48$ kHz, which overlaps with the measured dispersion. The spread of the data-points at small recoil values could originate from the thermal drift during the measurement.

Overall, we observe that detuning dependent excitation of avoided mode crossing are detrimental for the stability of the soliton Kerr comb, and cause an enhanced sensitivity of the soliton repetition rate to pump laser frequency fluctuations. At certain detuning points, the excitation of mode crossings causes abrupt changes in the comb repetition rate, resulting from the induced recoil, in agreement with simulations performed in [41]. The present method enables the identification of detuning regions that minimize the impact of avoided mode crossings. We also observed that the excitation of the strong avoided mode crossing at $\delta\omega/2\pi = 12$ MHz ($t \sim 450$ s) is correlated with a sudden shift of the \mathcal{S} -resonance toward lower frequency (see VNA map Fig. 3a). This is not yet understood and will be investigated further in another study.

At other detuning values $\delta\omega/2\pi =$

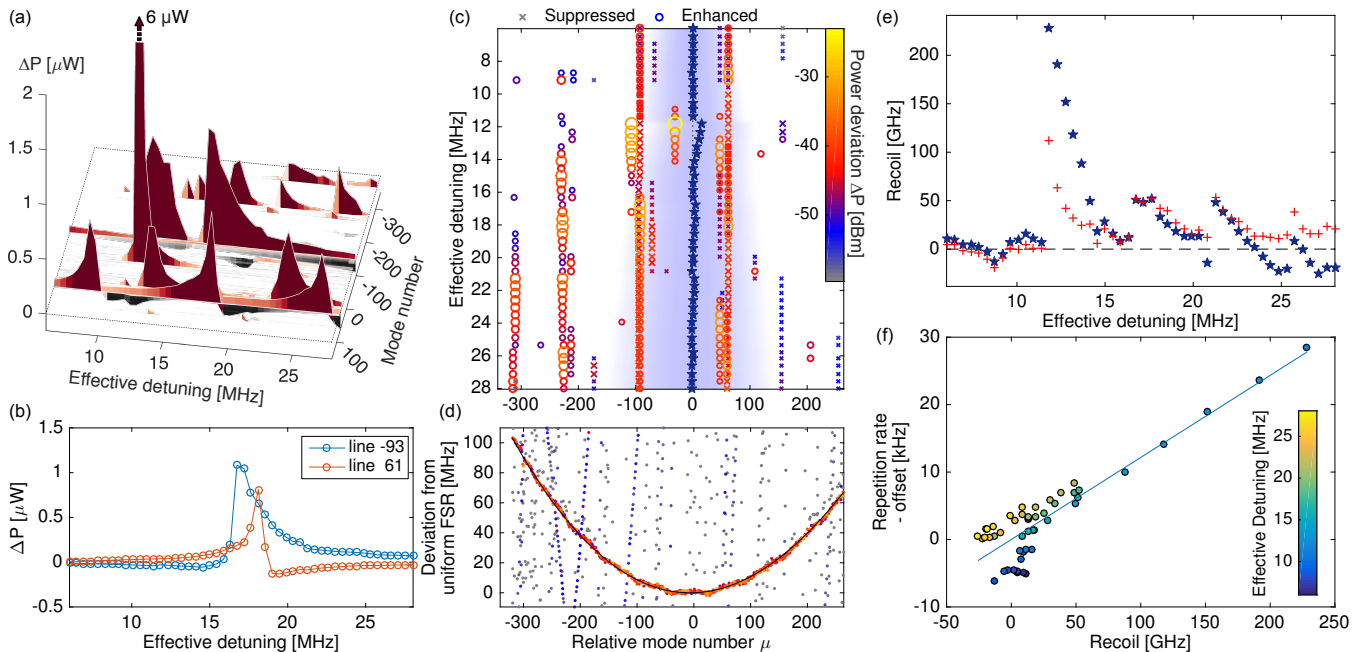


Figure 5. **Effect of detuning dependent avoided mode crossings on the soliton frequency comb.** (a) Map of ΔP indicating the spurs and dips in the spectrum after subtracting the fitted sech^2 soliton envelope. (b) Section of the ΔP map showing the evolution of the power deviation for the comb line +61 and -93 (relative to the pump) (c) Representation of the peaks in the ΔP map, in logarithmic units, showing the evolution of the intensity spurs caused by avoided mode crossings. The lines higher than the sech^2 envelope (enhanced) are marked with a dot, the lines lower (suppressed) with a cross. The blue stars mark the comb centroid Ω . The shaded blue region indicates the comb 3 dB width. When lines are strongly enhanced, the comb centroid shift away from them. (d) Measured frequency dispersion of the mode family supporting the soliton. A quadratic fit yields $D_1/2\pi = 14.0938$ GHz and $D_2/2\pi = 1.96$ kHz. Multiple mode families with a different FSR exist in the resonator and cross the family of interest, inducing small periodic disruptions on the dispersion. (e) Evolution of the soliton recoil. The blue stars result from the fit of the optical spectrum, while the red crosses mark the estimated recoil using (6). (f) The repetition rate frequency is strongly correlated with the recoil. This enables the determination of the dispersion parameter as given by the slope (D_2/D_1). The offset on the repetition rate is 14.094005 GHz.

15.5, 15.9, 17.2 MHz ($t \sim 750, 780, 880$ s), the \mathcal{S} -resonance peak appears greatly enhanced. This is concomitant with the appearance of sidebands around the repetition rate of the comb and of an amplitude modulation of the soliton pulse train at a frequency of ~ 3.5 MHz. These observations suggest that the soliton is breathing, meaning its amplitude and width oscillate in time, with a frequency typically much smaller than the repetition rate [42–45]. While such instabilities are known to occur for small detuning values [46, 47], they are unexpected for the large detuning values explored in the frame of this work. Our experiments suggest that the breathing of the soliton could be related and induced by the mode crossing feature at $\mu = -106$. This observation of mode crossing induced soliton breathing is reported here experimentally for the first time and will be further investigated in a future work.

Nevertheless, it is interesting to point out that our observations highlight the surprising robustness of the dispersive soliton, which is sustained in the cavity in spite of all the reported perturbations.

IV. DISCUSSION

We demonstrated a novel technique to probe, stabilize, and control the effective detuning of soliton states in optical microresonators via a feedback on the pump laser frequency. It enables the experimental study of the soliton’s properties while varying the effective detuning parameter and to verify the relation between this parameter and the soliton duration. This relation is surprisingly well preserved although the studied microresonator exhibits non-negligible deviations in its mode spectrum in the form of avoided mode crossings. In addition, we observed and studied the detuning-dependent mode crossing features and associated spectral recoil that correlates with a modification in the soliton round-trip time (repetition rate). These observations of a detuning dependent repetition rate have important repercussions for low phase noise microwave generation, as they enhance the transduction of pump laser frequency noise onto noise in the soliton pulse repetition rate. Furthermore, the mode crossings can also degrade the stability of the soliton and induce breathing in a region where solitons are expected

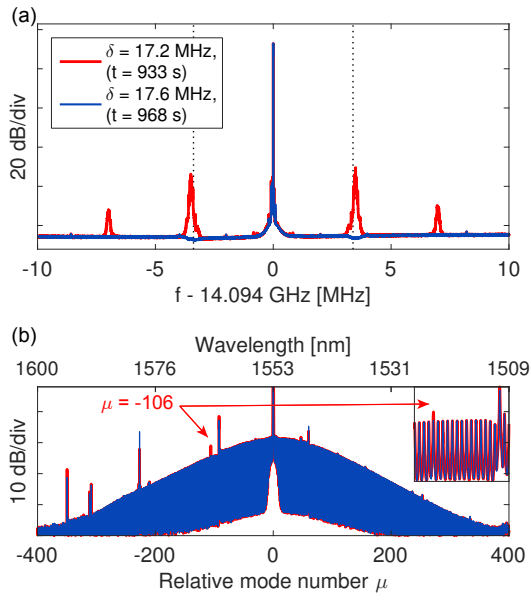


Figure 6. **Avoided mode crossing induced soliton breathing** (a) RF spectrum of the repetition rate for two adjacent detuning steps $\delta\omega/2\pi = 17.2$ and 17.6 MHz (resolution bandwidth 1 kHz). In the first case, modulations sidebands appear on the repetition beatnote, with a frequency of ~ 3.5 MHz, closely matching the S -resonance frequency measured on the VNA (indicated by the dashed lines). This is typically indicative of a soliton breathing. (b) Corresponding optical spectrum comparison. The red (blue) trace corresponds to the soliton breathing (stable). The breathing seems to correlate with the excitation of the mode $\mu = -106$.

to be stable.

Our method provides a way to experimentally explore the existence range of the soliton and identify optimal sets of operating parameters that favor a stable operation of the optical frequency comb. Moreover, we reveal how these crossings induce deviations in the relation between comb power and detuning, which can be a limitation for stabilization techniques based on the comb power alone [9, 48]. The presented method also enables the longterm

operation of soliton-based combs with stabilized bandwidth and power. The stabilization could alternatively be achieved by direct actuation on the microresonator [10, 49, 50], to tune the free spectral range and stabilize the cavity resonance on a stable pump laser. The fine control of the two driving parameters of the nonlinear system (detuning and pump power) will also enable the controlled access to various soliton regimes predicted by the theory (soliton breathers, chaos) [46]. The presented observations could also provide insights for sources of instabilities in systems described by the same type of driven, damped Nonlinear Schrödinger Equation, such as rf-driven waves in plasma [51], where similar probing and stabilization schemes could be applied.

Note: during submission of this work, Yi, et al., reported on the properties of single-mode dispersive waves induced by modal crossing [52].

ACKNOWLEDGMENTS

The authors acknowledge M. Gorodetsky for his fruitful discussions and suggestions, as well as M. Anderson, M. H. Pfeiffer, and V. Brasch for their valuable feedback on this paper. This work was supported by funding from the Swiss National Science Foundation under Grant Agreement No. 161573, as well as Contract No. W31P4Q-14-C-0050 (PULSE) from the Defense Advanced Research Projects Agency (DARPA), Defense Sciences Office (DSO). This material is based upon work supported by the Air Force Office of Scientific Research, Air Force Material Command, USAF under Award No. FA9550-15-1-0099. The authors acknowledge the support by the European Space Technology Centre with ESA Contracts No. 4000118777/16/NL/GM and No. 4000116145/16/NL/MH/GM, as well as funding from the European Union’s FP7 programme under Marie Skłodowska-Curie ITN Grant Agreement No. 607493 and the European Union’s Horizon 2020 research and innovation programme under Marie Skłodowska-Curie IF Grant Agreement No. 709249.

[1] F. Leo, S. Coen, P. Kockaert, S.-P. Gorza, P. Emplit, and M. Haelterman, *Nature Photonics* **4**, 471 (2010).
 [2] T. Herr, V. Brasch, J. D. Jost, C. Y. Wang, N. M. Kondratiev, M. L. Gorodetsky, and T. J. Kippenberg, *Nature Photonics* **8**, 145 (2013).
 [3] T. J. Kippenberg, R. Holzwarth, and S. A. Diddams, *Science* **332**, 555 (2011).
 [4] P. Del’Haye, A. Schliesser, O. Arcizet, T. Wilken, R. Holzwarth, and T. J. Kippenberg, *Nature* **450**, 1214 (2007).
 [5] S. Coen, H. G. Randle, T. Sylvestre, and M. Erkintalo, *Optics letters* **38**, 37 (2013).
 [6] A. B. Matsko, A. A. Savchenkov, W. Liang, V. S.

Ilchenko, D. Seidel, and L. Maleki, *Optics letters* **36**, 2845 (2011).
 [7] N. N. Akhmediev and A. Ankiewicz, “Solitons Around Us: Integrable, Hamiltonian and Dissipative Systems,” in *Optical Solitons: Theoretical and Experimental Challenges*, edited by K. Porsezian and V. C. Kuriakose (Springer Berlin Heidelberg, Berlin, Heidelberg, 2003) pp. 105–126.
 [8] V. Brasch, M. Geiselmann, T. Herr, G. Lihachev, M. H. P. Pfeiffer, M. L. Gorodetsky, and T. J. Kippenberg, *Science* **351**, 357 (2015).
 [9] X. Yi, Q.-F. Yang, K. Y. Yang, M.-G. Suh, and K. Vahala, *Optica* **2**, 1078 (2015).

- [10] C. Joshi, J. K. Jang, K. Luke, X. Ji, S. A. Miller, A. Klenner, Y. Okawachi, M. Lipson, and A. L. Gaeta, *Optics Letters* **41**, 2565 (2016).
- [11] P. Marin-Palomo, J. N. Kemal, M. Karpov, A. Kordts, J. Pfeifle, M. H. P. Pfeiffer, P. Trocha, S. Wolf, V. Brasch, R. Rosenberger, K. Vijayan, W. Freude, T. J. Kippenberg, and C. Koos, , 13 (2016), arXiv:1610.01484.
- [12] J. D. Jost, T. Herr, C. Lecaplain, V. Brasch, M. H. P. Pfeiffer, and T. J. Kippenberg, *Optica* **2**, 706 (2015).
- [13] P. Del’Haye, A. Coillet, T. Fortier, K. Beha, D. C. Cole, K. Y. Yang, H. Lee, K. J. Vahala, S. B. Papp, and S. A. Diddams, *Nature Photonics* **10**, 1 (2016).
- [14] V. Brasch, E. Lucas, J. D. Jost, M. Geiselmann, and T. J. Kippenberg, *Light Sci Appl.* **6**, e16202 (2017).
- [15] W. Liang, V. S. Ilchenko, D. Eliyahu, a. a. Savchenkov, a. B. Matsko, D. Seidel, and L. Maleki, *Nature Communications* **6**, 7371 (2015).
- [16] J. K. Jang, M. Erkintalo, S. G. Murdoch, and S. S. Coen, *Optics Letters* **39**, 5503 (2014).
- [17] N. Akhmediev and M. Karlsson, *Physical Review A* **51**, 2602 (1995).
- [18] S. Coen and M. Erkintalo, *Optics letters* **38**, 1790 (2013).
- [19] T. Carmon, L. Yang, and K. J. Vahala, *Optics Express* **12**, 4742 (2004).
- [20] P. Del’Haye, A. Coillet, W. Loh, K. Beha, S. B. Papp, S. A. Diddams, P. Del’Haye, A. Coillet, W. Loh, K. Beha, S. B. Papp, and S. A. Diddams, *Nature Communications* **6**, 1 (2015).
- [21] A. B. Matsko and L. Maleki, *Physical Review A* **91**, 013831 (2015).
- [22] H. Guo, M. Karpov, E. Lucas, A. Kordts, M. H. P. Pfeiffer, V. Brasch, G. Lihachev, V. E. Lobanov, M. L. Gorodetsky, and T. J. Kippenberg, *Nature Physics* **13**, 94 (2017).
- [23] T. Herr, K. Hartinger, J. Riemensberger, C. Y. Wang, E. Gavartin, R. Holzwarth, M. L. Gorodetsky, and T. J. Kippenberg, *Nature Photonics* **6**, 480 (2012).
- [24] Y. K. Chembo and C. R. Menyuk, *Phys. Rev. A* **87**, 053852 (2013).
- [25] S. Wabnitz, *Opt. Lett.* **18**, 601 (1993).
- [26] L. A. Lugiato and R. Lefever, *Physical review letters* **58**, 2209 (1987).
- [27] J. K. Wahlstrand, J. T. Willits, T. R. Schibli, C. R. Menyuk, and S. T. Cundiff, *Optics Letters* **32**, 3426 (2007).
- [28] C. C. Lee and T. R. Schibli, *Physical Review Letters* **112**, 223903 (2014).
- [29] T. Herr, V. Brasch, J. D. Jost, I. Mirgorodskiy, G. Lihachev, M. L. Gorodetsky, and T. J. Kippenberg, *Physical Review Letters* **113**, 123901 (2014).
- [30] P. Del’Haye, O. Arcizet, M. L. Gorodetsky, R. Holzwarth, and T. J. Kippenberg, *Nature Photonics* **3**, 529 (2009).
- [31] I. S. Grudin, L. Baumgartel, and N. Yu, *Optics express* **21**, 26929 (2013).
- [32] H. Zhou, S. W. Huang, Y. Dong, M. Liao, K. Qiu, and C. W. Wong, *IEEE Photonics Journal* **7**, 1 (2015).
- [33] C. Milián and D. V. Skryabin, *Optics Express* **22**, 3732 (2014).
- [34] A. B. Matsko, W. Liang, A. A. Savchenkov, D. Eliyahu, and L. Maleki, *Optics Letters* **41**, 2907 (2016).
- [35] Y. Wang, F. Leo, J. Fatome, K. Luo, J. K. Jang, M. J. Erkintalo, S. G. Murdoch, and S. Coen, in *Conference on Lasers and Electro-Optics*, OSA Technical Digest (online) (Optical Society of America, San Jose, California, 2016) p. FF2A.6.
- [36] M. Karpov, H. Guo, A. Kordts, V. Brasch, M. H. P. Pfeiffer, M. Zervas, M. Geiselmann, and T. J. Kippenberg, *Physical Review Letters* **116**, 103902 (2016).
- [37] S. P. S. Porto, P. A. Fleury, and T. C. Damen, *Physical Review* **154**, 522 (1967).
- [38] Q.-F. Yang, X. Yi, K. Y. Yang, and K. Vahala, *Optica* **3**, 1132 (2016).
- [39] R. Paschotta, *Applied Physics B* **79**, 163 (2004).
- [40] H. a. Haus and A. Mecozzi, *IEEE Journal of Quantum Electronics* **29**, 983 (1993).
- [41] A. B. Matsko, Wei Liang, V. S. Ilchenko, A. A. Savchenkov, J. Byrd, D. Seidel, and L. Maleki, in *2014 IEEE Photonics Conference* (IEEE, 2014) pp. 108–109.
- [42] A. Matsko, A. Savchenko, and L. Maleki, *Opt. Lett.* **37**, 4856 (2012).
- [43] M. Yu, J. K. Jang, Y. Okawachi, A. G. Griffith, K. Luke, S. A. Miller, X. Ji, M. Lipson, and A. L. Gaeta, , 1 (2016), arXiv:1609.01760.
- [44] E. Lucas, M. Karpov, H. Guo, M. Gorodetsky, and T. Kippenberg, , 10 (2016), arXiv:1611.06567.
- [45] C. Bao, J. A. Jaramillo-Villegas, Y. Xuan, D. E. Leaird, M. Qi, and A. M. Weiner, *Physical Review Letters* **117**, 163901 (2016).
- [46] F. Leo, L. Gelens, P. Emplit, M. Haelterman, and S. Coen, *Optics express* **21**, 9180 (2013).
- [47] M. Anderson, F. Leo, S. Coen, M. Erkintalo, and S. G. Murdoch, *Optica* **3**, 1071 (2016).
- [48] X. Yi, Q.-F. Yang, K. Youl, and K. Vahala, *Optics Letters* **41**, 2037 (2016).
- [49] J. D. Jost, E. Lucas, T. Herr, C. Lecaplain, V. Brasch, M. H. P. Pfeiffer, and T. J. Kippenberg, *Optics Letters* **40**, 4723 (2015).
- [50] S. B. Papp, P. Del’Haye, and S. A. Diddams, *Physical Review X* **3**, 031003 (2013).
- [51] K. Nozaki and N. Bekki, *Physica D: Nonlinear Phenomena* **21**, 381 (1986).
- [52] X. Yi, Q.-F. Yang, X. Zhang, K. Y. Yang, and K. Vahala, , 1 (2016), arXiv:1610.08145.